American Mineralogist, Volume 95, pages 1408–1412, 2010

$(H_3O)Fe(SO_4)_2$ formed by dehydrating rhomboclase and its potential existence on Mars

Wenqian Xu,[1,*] John B. Parise,[1,2] and Jonathan Hanson[3]

[1]Department of Geosciences, Stony Brook University, Stony Brook, New York 11794-2100, U.S.A.
[2]Department of Chemistry, Stony Brook University, Stony Brook, New York 11794-3400, U.S.A.
[3]Department of Chemistry, Brookhaven National Laboratory, Upton, New York, 11793-5000, U.S.A.

Abstract

Rhomboclase, $(H_5O_2)Fe(SO_4)_2\cdot 2H_2O$, transforms to a solid crystalline phase, $(H_3O)Fe(SO_4)_2$, upon dehydration. The structure of $(H_3O)Fe(SO_4)_2$ is found to be the same as a recently reported structure determined from single-crystal diffraction by Peterson et al. (2009), who synthesized the same compound using a hydrothermal method. The phase boundary between rhomboclase and $(H_3O)Fe(SO_4)_2$ as a function of temperature (*T*) and relative humidity (RH) was determined by environment-controlled in situ X-ray diffraction (XRD) method. The stability of $(H_3O)Fe(SO_4)_2$ against rhomboclase was further evaluated under a simulated martian condition (constant 50% RH, –20 °C, 6 mbar CO_2). Both phases remained after 14 days with no observable transition. This result suggests that hydrate ferric sulfate minerals might not respond to diurnal RH fluctuation under the extremely slowed kinetics expected on the martian surface.

Keywords: Rhomboclase, sulfate, hydrate, humidity, Mars, ferric sulfate

Introduction

Rhomboclase, $(H_5O_2)Fe(SO_4)_2\cdot 2H_2O$, a common secondary iron sulfate mineral found in acid mine drainage (AMD) regions (Nordstrom and Alpers 1999; Jambor et al. 2000; Keith et al. 2001; Buckby et al. 2003; Hammarstrom et al. 2005), has also been suggested as a potential hydrated iron sulfate in the sulfur-rich soils at Gusev Crater on Mars (Johnson et al. 2007; Lane et al. 2008; Yen et al. 2008). In laboratory studies, rhomboclase was found in evaporites of a brine from chemically weathering synthetic martian basalts (Tosca et al. 2004; Hurowitz et al. 2005; Tosca and McLennan 2009). Iron sulfates are sensitive to environmental changes such as relative humidity (RH) and *T* and can thus act as mineral indicators of current and past sedimentary environments. Precipitates from aqueous Fe(III)-SO_4-H_2O systems have been previously studied (King and McSween 2005; Jonsson et al. 2006; Tosca et al. 2007; Marion et al. 2008). Rhomboclase precipitates at pH ≤ –1.8 (Marion et al. 2008), lower than the pH for ricopiapite $[Fe_{4.67}(SO_4)_6(OH)_2\cdot 20H_2O]$ precipitation (–1 < pH < 1) and jarosite $[(K,Na,H_3O)Fe_3(OH)_6(SO4)_2]$ precipitation (1 < pH < 3) (Jonsson et al. 2006; Tosca et al. 2008). Though primarily precipitating at different pH conditions, the laboratory study has shown rhomboclase and ferricopiapite can co-precipitate by evaporation of a ferric sulfate solution (molar ratio $Fe^{3+}/SO_4^{2-} = 2/3$) (Xu et al. 2009). The mixture of rhomboclase and ferricopiapite may combine to form kornelite $[Fe_2(SO_4)_3\cdot 7.25H_2O]$ and paracoquimbite $[Fe_2(SO_4)_3\cdot 9H_2O]$ in the diagenesis process (Xu et al. 2009). Conversion of ferricopiapite to rhomboclase was also observed during the dehydration of ferricopiapite, probably due to a subtle change of environmental acidity (Freeman et al. 2009). Thermodynamic data for these iron sulfates are recently reported by J. Majzlan and colleagues (Majzlan et al. 2004, 2005, 2006; Ackermann et al. 2009) and these data help understand the phase stability relations in the Fe(III)-SO_4-H_2O system. Here we evaluate the stability of rhomboclase with changes of RH and *T*, and find a transition to a dehydrated phase, $(H_3O)Fe(SO_4)_2$. Powder XRD shows the dehydrated phase has the same structure as that recently reported from a single crystal $(H_3O)Fe(SO_4)_2$ (Peterson et al. 2009), synthesized hydrothermally at 140 °C. Further experiments under simulated martian conditions suggested the dehydrated phase may exist on the current martian surface.

Experimental methods

Synthesis

Rhomboclase was synthesized according to methods described in the literature (Majzlan et al. 2006): mixing 2 g of anhydrous ferric sulfate, 2.5 g of water, and 2.5 g of sulfuric acid (95.9% H_2SO_4 by mass) to produce a solution. Anhydrous ferric sulfate was made by baking ferric sulfate hydrate [Baker Analyzed, Assay $Fe_2(SO_4)_3 > 73.0\%$] at 300 °C for 2 h to remove all the water content. XRD analysis confirmed the product of this treatment was pure trigonal $Fe_2(SO_4)_3$. The solution was evaporated at ambient conditions (20 °C, 10–30% RH). A white solid forming after three days was confirmed as rhomboclase by XRD. The product was vacuum-filtered and rinsed with deionized water and ethanol to remove any surface H_2SO_4. The yield was calculated as 68% based on the amount of Fe used in the synthesis.

Thermal analysis

Thermogravimetric and differential scanning calorimetric analysis (TG and DSC) was performed on a Netzsch STA 449C Jupiter simultaneous TG-DSC apparatus. A 7.7 mg powdered sample of freshly prepared rhomboclase was loaded in an alumina crucible with a hole in the cover and heated from room temperature to 300 °C at a rate of 3 °C/min under N_2 flow.

* E-mail: wenqian.xu@stonybrook.edu

T-resolved XRD

In situ synchrotron XRD data were collected at the X7B beamline at the National Synchrotron Light Source, to follow the dehydration of rhomboclase under rising *T*. Sample powders were loaded into Kapton polyimide capillaries with a 0.5 mm inner diameter. The X-ray beam height was matched to capillary diameter using variable slits. An air-blower type heater was used to control the temperature with the control thermocouple placed in contact with the outside of the capillary (Norby 1996). The heater was programmed to heat in a range from 30 to 180 °C at a rate of 1 °C/min. XRD data were collected continuously on a MAR345 2-dimensional detector with 120 s exposure time, plus 80 s readout time before the start of the next exposure. The time resolution was 200 s per exposure for the series diffraction patterns. The sample-to-detector distance, X-ray beam center, and the tilt of the detector relative to the incident beam were calibrated using a standard LaB_6. The X-ray wavelength used was 0.31840(4) Å. The collected 2-D raw data were converted to traditional intensity vs. 2θ plot using the program Fit2D (Hammersley et al. 1996). RH was not controlled in this experiment.

RH-resolved DSC-XRD

To investigate the combined effects of both RH and *T* on rhomboclase stability, in situ powder diffraction data were collected on a Rigaku Ultima-IV diffractometer with a built-in environmental chamber and devices to control both *T* and RH (Kishi and Toraya 2004). Cu*K*α radiation (λ = 1.5406 Å) was used in conjunction with a high-speed semiconductor element one-dimensional X-ray detector capable of energy discrimination to eliminate the effect of Fe fluorescence in this experiment. The same sample stage used for environment control also allowed DSC measurement. In preparation of a specimen, sample powder was spread onto a $7 \times 7 \times 0.25$ mm aluminum pan. The sample pan was placed onto the DSC heating stage beside a DSC reference pan. The DSC data were less sensitive compared to the TG-DSC apparatus due to the smaller sample size used and the open crucible necessitated by the simultaneous XRD measurement.

During the experiment, *T* was maintained at several arbitrary values between room *T* to 95 °C. At each *T*, RH was varied at a rate of 0.1% per min to cross the phase boundary from both sides. Five cartridge heaters placed in the wall of the sample chamber helped maintain a homogeneous thermal field inside. The thermocouple measuring the chamber *T* and the thermocouple below the sample pan indicated a *T* gradient of <1 °C. This is important since RH is strongly temperature dependent. XRD data were collected repeatedly spanning a 2θ range from 8 to 14° within a scan rate of 6 °/min. This 2θ range covers reflection (020) of rhomboclase and reflection (010) of the $(H_3O)Fe(SO_4)_2$ that are the most intense peaks of each phase.

Without using a RH control, DSC-XRD experiment on the thermal decomposition of rhomboclase was also performed on Ultima-IV using a heating rate of 1 °C/min to 225 °C under N_2 flow.

Simulating martian conditions

Minerals on the martian surface are exposed to an atmosphere consisting mainly of CO_2 with about 6 mbar pressure. A good simulation of the martian atmosphere can be achieved using a simple vacuum line, with powder samples loaded into glass ampoules that can be attached and detached. To simulate martian surface conditions, the whole system was first evacuated and then filled with 6.1 mbar CO_2 and 0.8 mbar water vapor at room *T* (20 °C), which would create an atmosphere with 50% RH and 6 mbar atmospheric pressure at –20 °C. The sample container was then closed, disconnected from the vacuum line, and kept in a freezer set at –20 °C. Because it is a sealed system, the RH in the container will drop or rise when water vapor is absorbed to or released from the sample. To maintain a constant RH and make it more like an open system, the sample container was briefly reconnected to the vacuum line each day and allowed to equilibrate the water vapor concentration. After 14 days, the samples were taken out and their XRD patterns were taken at ambient conditions (21 °C, 23% RH). There was about a 3 min exposure of the sample to atmosphere for transporting the samples to the diffractometer and collecting XRD data; it turned out this short exposure did not affect the speciation of the sample (see below).

Results and Discussion

Thermal decomposition of rhomboclase

TG and DSC. Figure 1 shows the TG and DSC profiles for rhomboclase. Three endothermic events were recorded at 91, 150, and 195 °C, respectively. The first endotherm corresponded to a 17% weight loss, equal to the weight ratio of 3 H_2O molecules over rhomboclase: $3\times M_{H_2O}/M_{(H_5O_2)Fe(SO_4)_2\cdot 2H_2O} = 16.8\%$. The compound after this dehydration step would have a nominal formula as $(H_3O)Fe(SO_4)_2$. This formula was later confirmed by the structural information obtained from in situ XRD data (see below). The second and third endotherms were overlapping with each other and the sample weight dropped continuously to 63.5% of the initial weight. The final product was monoclinic $Fe_2(SO_4)_3$ according to XRD. This is consistent with the TG result: $M_{Fe_2(SO_4)_3}/2\times M_{(H_5O_2)Fe(SO_4)_2\cdot 2H_2O} = 62.3\%$. The reactions happening at the second step of weight loss could be written as:

$$2\,(H_3O)Fe(SO_4)_2 \rightarrow Fe_2(SO_4)_3 + 2H_2O(g) + H_2(SO)_4.$$

This is both a dehydration and a desulfation process. The endotherm at 150 °C corresponds to the decomposition of $(H_3O)Fe(SO_4)_2$ to $Fe_2(SO_4)_3$, as confirmed by DSC-XRD data (see below). No solid phase transition occurred during the third thermal event at 195 °C, but a continuous weight drop was recorded in TG. This is most likely due to the evaporation of sulfuric acid. Enthalpies of transition were calculated from the DSC data by integrating peak areas: –478.9, –164.1, and –134.9 J/g for the three thermal events from low to high temperature.

In situ *T*-resolved synchrotron XRD. *T*-resolved XRD data on heating rhomboclase revealed a two-step structure change at 73 and 128 °C, shown in Figure 2. The intermediate phase between 73 and 128 °C was found to be $(H_3O)Fe(SO_4)_2$ according to XRD (Peterson et al. 2009). At 128 °C, $(H_3O)Fe(SO_4)_2$ decomposed to monoclinic $Fe_2(SO_4)_3$.

DSC-XRD data. Figure 3 shows the laboratory XRD series recording the thermal decomposition of rhomboclase along with the simultaneously collected DSC data. The same two-step transformation from rhomboclase to $(H_3O)Fe(SO_4)_2$ and then to monoclinic $Fe_2(SO_4)_3$ was revealed from XRD. Correspondingly, two endotherms at 95 and 157 °C were recorded in the DSC data at each transition point. A concave upward shape of the DSC curve between 150 and 190 min was probably due to the evaporation of $H_2(SO)_4$, that also caused the 195 °C endotherm in Figure 2. The shape difference was possibly caused by different DSC settings (see Experimental Methods).

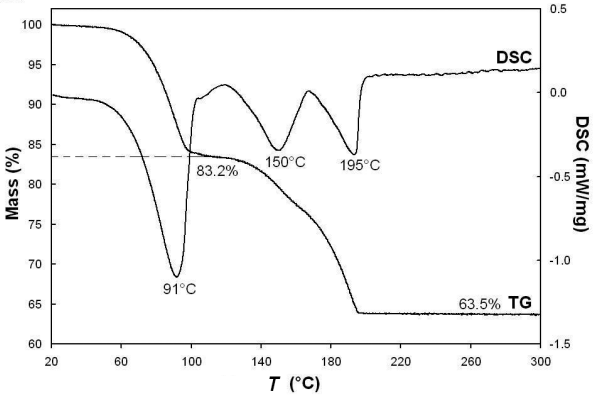

Figure 1. TG and DSC data of rhomboclase.

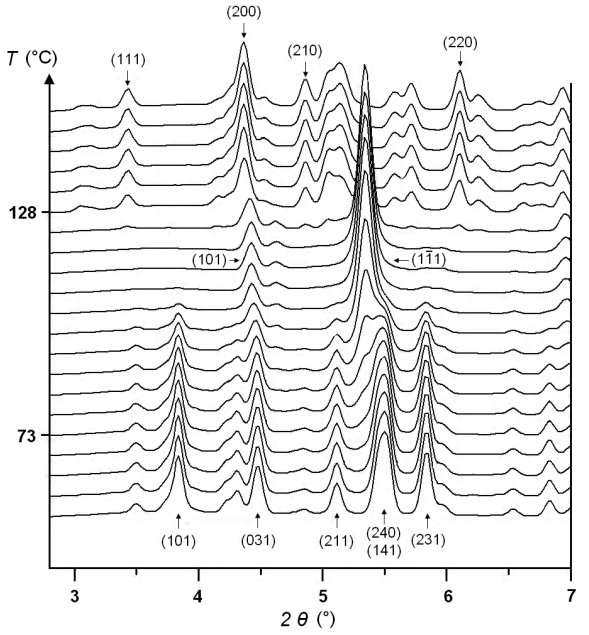

FIGURE 2. *T*-resolved synchrotron XRD data showing the thermal decomposition of rhomboclase to $(H_3O)Fe(SO_4)_2$ then to monoclinic $Fe_2(SO_4)_3$. Some reflections are indexed for rhomboclase at the bottom, $(H_3O)Fe(SO_4)_2$ in the middle, and monoclinic $Fe_2(SO_4)_3$ at the top.

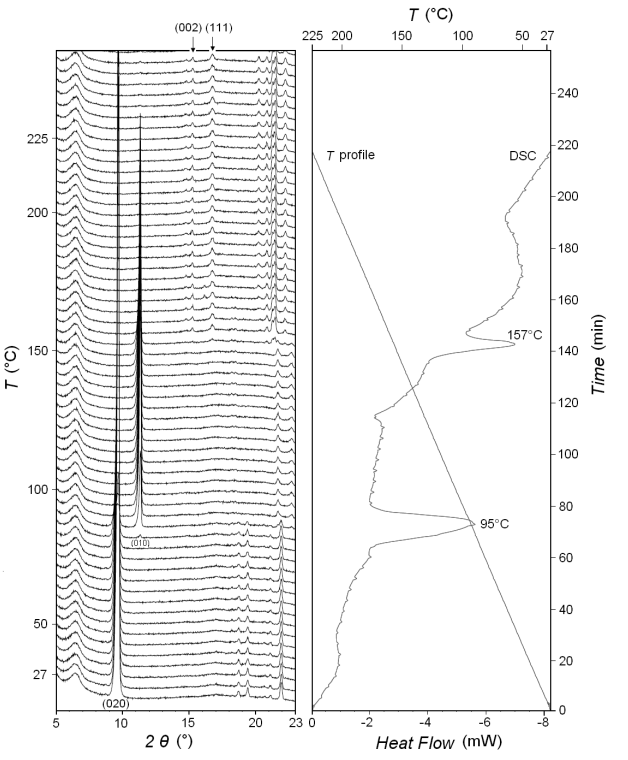

FIGURE 3. DSC-XRD data showing the thermal decomposition of rhomboclase to $(H_3O)Fe(SO_4)_2$ and to monoclinic $Fe_2(SO_4)_3$.

RH-*T* phase diagram

A phase diagram showing the stability of rhomboclase and $(H_3O)Fe(SO_4)_2$ as a function of RH and *T* is plotted in Figure 4. Each data point was obtained from an RH-resolved DSC-XRD experiment, in which the dehydration or hydration was induced by varying RH while maintaining a constant temperature. Figure 5 shows the RH-induced dehydration of rhomboclase to $(H_3O)Fe(SO_4)_2$ at 72 °C. The transition to $(H_3O)Fe(SO_4)_2$ happened at 8% RH, as recorded by XRD and DSC. Each transition RH with the corresponding *T* is listed in Table 1. Notice in Figure 4 that there appears to be a hysteresis between the hydration RH and dehydration RH: the hydration RH is higher than the dehydration RH at the same *T*. The equilibrium RH should be within the domain confined by the measured points. The expected phase boundary is drawn in Figure 4.

Rhomboclase is commonly found in AMD regions, usually under very acidic conditions where pH could be as low as –3.6 (Nordstrom et al. 2000). But the dehydrated phase was never reported. This is expectable from the phase diagram (Fig. 4) where RH is required to reach 2–4% or below to favor the transformation to the dehydrated phase at 20–50 °C. Such dry condition is not normally found in AMD regions. However, the dehydrated phase may still be present at high-temperature spots, like close to fumaroles or under burial conditions. A good example is mikasaite, trigonal $(Fe,Al)_2(SO_4)_3$, an extremely hygroscopic mineral. It was discovered around coal gas escape fractures, where temperature was around 300 °C to keep the mineral from absorbing H_2O (Miura et al. 1994).

Also mapped in Figure 4 is the deliquescence boundary of rhomboclase. Rhombolcase is dissolved when RH reaches 60–65% at 25–40 °C. The dissolution releases hydronium ions

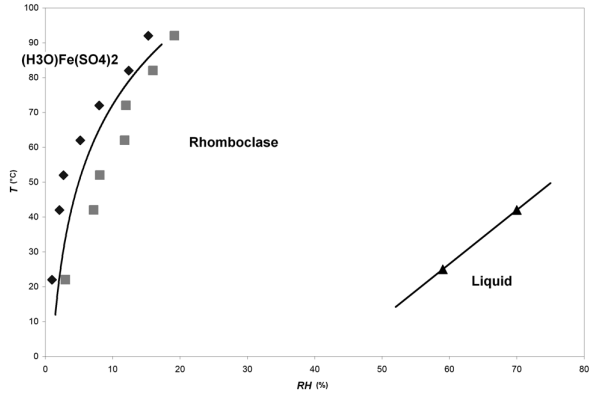

FIGURE 4. RH-*T* phase diagram of rhomboclase. Diamond spot represents the dehydration (RH, *T*) of rhomboclase; square represents the hydration (RH, *T*) of $(H_3O)Fe(SO_4)_2$; triangle represents the deliquescence (RH, *T*) of rhomboclase.

that will acidify the stream. Other ferric sulfate minerals also produce acid when dissolved because of Fe^{3+} hydrolysis, though not as strong as rhomboclase. Other than acidity, the released metal ions like Fe^{3+}, Zn^{2+}, and Cu^{2+} also contaminate the aquatic system. The water quality is worse in humid seasons than in dry seasons due to the dissolution of these efflorescent minerals (Hammarstrom et al. 2005). Mapping the deliquescence boundary for these sulfate minerals will be useful in predicting local water quality combined with a weather forecast.

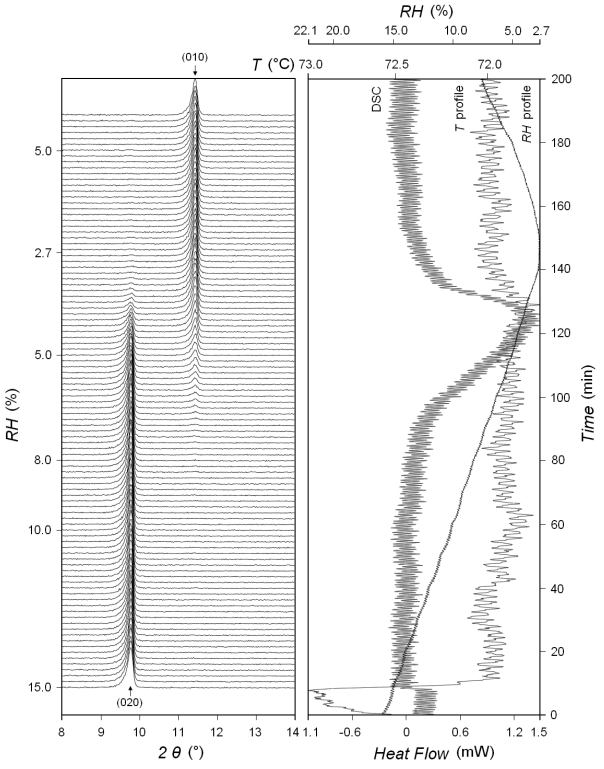

FIGURE 5. DSC-XRD data showing the RH-induced dehydration of rhomboclase to $(H_3O)Fe(SO_4)_2$ at 72 °C.

Stability under simulated martian condition

Both rhomboclase and the dehydrated samples were stored for 14 days under the simulated conditions of the martian surface, 6 mbar air pressure, 50% RH, and –20 °C. Neither was rhomboclase detected in the $(H_3O)Fe(SO_4)_2$ sample from XRD, nor was $(H_3O)Fe(SO_4)_2$ found in the rhomboclase sample. According to the RH-*T* phase diagram as shown in Figure 4, the experimental condition (–20 °C, 50% RH) should fall into the rhomboclase stability region, assuming the phase boundary line can be extrapolated to below 0 °C. So the absence of rhomboclase in the $(H_3O)Fe(SO_4)_2$ sample may be due to the extremely slow kinetics at –20 °C. Also, the absence of rhomboclase indicated there was little influence of the short exposure to the atmosphere during the XRD measurement, as the ambient condition (21 °C, 23% RH) was supposed to favor the transformation to rhomboclase. Even though this experimental result did not confirm which species was more favored in the conditions used to simulate the martian surface, it provided a lower limit of how slow the hydration or dehydration might be on Mars. Therefore, rhomboclase, or $(H_3O)Fe(SO_4)_2$, if present on the surface of Mars, will not respond to the diurnal fluctuation of RH, e.g., RH varies from <1 to 100% at the Viking Lander 1 site during summertime (Savijarvi 1995). The suggestion that low *T* on Mars can dramatically slow down the kinetics is also supported by spectroscopic observations that sulfate deposits in East Candor did not show changes in hydration state over 2 years (Roach et al. 2009).

TABLE 1. Experimental transition RH and *T* between rhomboclase and $(H_3O)Fe(SO_4)_2$ and the deliquescence RH of rhomboclase

T (±1 °C)	RH (±1.0%)		
	Dehydration	Hydration	Deliquescence
22	1.0	3.0	59.2
42	2.1	7.2	70.5
52	2.7	8.1	
62	5.2	11.8	
72	8.0	12.0	
82	12.4	16.0	
92	15.3	19.2	

In summary, we used the combined RH-DSC-XRD method to study the thermal stability of rhomboclase, found a transformation to $(H_3O)Fe(SO_4)_2$ at high-*T* or low-RH conditions, and mapped the RH-*T* phase diagram. The successful application of the DSC-XRD technique provided a promising future for its use in exploring mineral stability and phase transition, in case complex heat signatures need to be deconvolved and correlated with structural changes.

ACKNOWLEDGMENTS

The authors appreciate Juraj Majzlan and an anonymous reviewer's helpful comments to strengthen the manuscript. The authors also appreciate the support from NASA grant MFRP07-0022. Part of this research was carried out at the National Synchrotron Light Source, Brookhaven National Laboratory, supported by the U.S. Department of Energy, Division of Materials Sciences and Division of Chemical Sciences, through contract no. DE-AC02-98CH10886.

REFERENCES CITED

Ackermann, S., Lazic, B., Armbruster, T., Doyle, S., Grevel, K.D., and Majzlan, J. (2009) Thermodynamic properties of kornelite $[Fe_2(SO_4)_3 \cdot 7.75H_2O]$ and paracoquimbite $[Fe_2(SO_4)_3 \cdot 9H_2O]$. American Mineralogist, 94, 1620–1628.

Buckby, T., Black, S., Coleman, M.L., and Hodson, M.E. (2003) Fe-sulphate-rich evaporative mineral precipitates from the Rio Tinto, southwest Spain. Mineralogical Magazine, 67, 263–278.

Freeman, J.J., Wang, A., and Ling, Z.C. (2009) Ferric sulfates on Mars: Mission observations and laboratory investigations. Lunar and Planetary Science XL, March 23–27, The Woodlands, Texas, abstract 2284.

Hammarstrom, J.M., Seal, R.R., Meier, A.L., and Kornfeld, J.M. (2005) Secondary sulfate minerals associated with acid drainage in the eastern U.S.: Recycling of metals and acidity in surficial environments. Chemical Geology, 215, 407–431.

Hammersley, A.P., Svensson, S.O., Hanfland, M., Fitch, A.N., and Hausermann, D. (1996) Two-dimensional detector software: From real detector to idealised image or 2 scan. High Pressure Research, 14, 235–248.

Hurowitz, J.A., McLennan, S.M., Lindsley, D.H., and Schoonen, M.A.A. (2005) Experimental epithermal alteration of synthetic Los Angeles meteorite: Implications for the origin of Martian soils and identification of hydrothermal sites on Mars. Journal of Geophysical Research-Planets, 110, E07002, DOI: 10.1029/2004JE002391.

Jambor, J.I., Nordstrom, D.K., and Alpers, C.N. (2000) Metal-sulfate salts from sulfide mineral oxidation. In C.N. Alpers, J.L. Jambor, D.K. Nordstrom, Eds., Sulfate Minerals—Crystallography, Geochemistry, and Environmental Significance, 40, p. 303–350. Reviews in Mineralogy and Geochemistry, Mineralogical Society of America, Chantilly, Virginia.

Johnson, J.R., Bell, J.F., Cloutis, E., Staid, M., Farrand, W.H., McCoy, T., Rice, M., Wang, A., and Yen, A. (2007) Mineralogic constraints on sulfur-rich soils from Pancam spectra at Gusev crater, Mars. Geophysical Research Letters, 34, L13202, DOI: 10.1029/2007GL029894.

Jonsson, J., Jonsson, J., and Lovgren, L. (2006) Precipitation of secondary Fe(III) minerals from acid mine drainage. Applied Geochemistry, 21, 437–445.

Keith, D.C., Runnells, D.D., Esposito, K.J., Chermak, J.A., Levy, D.B., Hannula, S.R., Watts, M., and Hall, L. (2001) Geochemical models of the impact of acidic groundwater and evaporative sulfate salts on Boulder Creek at Iron Mountain, California. Applied Geochemistry, 16, 947–961.

King, P.L. and McSween, H.Y. (2005) Effects of H_2O, pH, and oxidation state on the stability of Fe minerals on Mars. Journal of Geophysical Research-Planets, 110, E12S10, DOI: 10.1029/2005JE002482.

Kishi, A. and Toraya, H. (2004) Simultaneous measurements of X-ray diffraction (XRD) and differential scanning calorimetry (DSC) data under controlled humidity condition: Instrumentation and application to studies on hydration, dehydration, and rehydration processes of pharmaceutical compounds. Powder

Diffraction, 19, 31–35.
Lane, M.D., Bishop, J.L., Dyar, M.D., King, P.L., Parente, M., and Hyde, B.C. (2008) Mineralogy of the Paso Robles soils on Mars. American Mineralogist, 93, 728–739.
Majzlan, J., Stevens, R., Boerio-Goates, J., Woodfield, B.F., Navrotsky, A., Burns, P.C., Crawford, M.K., and Amos, T.G. (2004) Thermodynamic properties, low-temperature heat-capacity anomalies, and single-crystal X-ray refinement of hydronium jarosite, $(H_3O)Fe_3(SO_4)_2(OH)_6$. Physics and Chemistry of Minerals, 31, 518–531.
Majzlan, J., Navrotsky, A., Stevens, R., Donaldson, M., Woodfield, B.F., and Boerio-Goates, J. (2005) Thermodynamics of monoclinic $Fe_2(SO_4)_3$. Journal of Chemical Thermodynamics, 37, 802–809.
Majzlan, J., Navrotsky, A., McCleskey, R.B., and Alpers, C.N. (2006) Thermodynamic properties and crystal structure refinement of ferricopiapite, coquimbite, rhomboclase, and $Fe_2(SO_4)_3(H_2O)_5$. European Journal of Mineralogy, 18, 175–186.
Marion, G.M., Kargel, J.S., and Catling, D.C. (2008) Modeling ferrous-ferric iron chemistry with application to martian surface geochemistry. Geochimica et Cosmochimica Acta, 72, 242–266.
Miura, H., Niida, K., and Hirama, T. (1994) Mikasaite, $(Fe, Al)_2(SO_4)_3$, a new ferric sulfate mineral from Mikasa City, Hokkaido, Japan. Mineralogical Magazine, 58, 649–653.
Norby, P. (1996) In-situ time resolved synchrotron powder diffraction studies of syntheses and chemical reactions. European Powder Diffraction 4, Materials Science Forum, 228–231, 147–152.
Nordstrom, D.K. and Alpers, C.N. (1999) Negative pH, efflorescent mineralogy, and consequences for environmental restoration at the Iron Mountain Superfund site, California. Proceedings of the National Academy of Sciences, 96, 3455–3462.
Nordstrom, D.K., Alpers, C.N., Ptacek, C.J., and Blowes, D.W. (2000) Negative pH and extremely acidic mine waters from Iron Mountain, California. Environmental Science and Technology, 34, 254–258.
Peterson, R.C., Valyashko, E., and Wang, R.Y. (2009) The atomic structure of $(H_3O)Fe(SO_4)_2$ and rhombolcase, $(H_5O_2)Fe(SO_4)_2 \cdot 2H_2O$. Canadian Mineralogist, 47, 625–634.
Roach, L.H., Mustard, J.F., Murchie, S.L., Bibring, J.P., Forget, F., Lewis, K.W., Aharonson, O., Vincendon, M., and Bishop, J.L. (2009) Testing evidence of recent hydration state change in sulfates on Mars. Journal of Geophysical Research-Planets, 114, E00D02, DOI: 10.1029/2008JE003245.
Savijarvi, H. (1995) Mars boundary-layer modeling—diurnal moisture cycle and soil properties at the Viking-Lander-1 site. Icarus, 117, 120–127.
Tosca, N.J. and McLennan, S.M. (2009) Experimental constraints on the evaporation of partially oxidized acid-sulfate waters at the martian surface. Geochimica et Cosmochimica Acta, 73, 1205–1222.
Tosca, N.J., McLennan, S.M., Lindsley, D.H., and Schoonen, M.A.A. (2004) Acid-sulfate weathering of synthetic Martian basalt: The acid fog model revisited. Journal of Geophysical Research-Planets, 109, E05003, DOI: 10.1029/2003JE002218.
Tosca, N.J., Smirnov, A., and McLennan, S.M. (2007) Application of the Pitzer ion interaction model to isopiestic data for the $Fe_2(SO_4)_3$-H_2SO_4-H_2O system at 298.15 and 323.15 K. Geochimica et Cosmochimica Acta, 71, 2680–2698.
Tosca, N.J., McLennan, S.M., Dyar, M.D., Sklute, E.C., and Michel, F.M. (2008) Fe oxidation processes at Meridiani Planum and implications for secondary Fe mineralogy on Mars. Journal of Geophysical Research-Planets, 113, E05005, DOI: 10.1029/2007JE003019.
Xu, W., Tosca, N., McLennan, S.M., and Parise, J.B. (2009) Humidity-induced phase transitions of ferric sulfate minerals studied by in situ and ex situ X-ray diffraction. American Mineralogist, 94, 1629–1637.
Yen, A.S., Morris, R.V., Clark, B.C., Gellert, R., Knudson, A.T., Squyres, S., Mittlefehldt, D.W., Ming, D.W., Arvidson, R., McCoy, T., Schmidt, M., Hurowitz, J., Li, R., and Johnson, J.R. (2008) Hydrothermal processes at Gusev Crater: An evaluation of Paso Robles class soils. Journal of Geophysical Research-Planets, 113, E06S10, DOI: 10.1029/2007JE002978.

Manuscript received December 4, 2009
Manuscript accepted June 3, 2010
Manuscript handled by Matthias Gottschalk